Journal of Metals, Materials and Minerals, 36(3), e2396, 2026

Mechanical and microstructural characterization of TiB_2/ZrO_2 reinforced Al5052 nanocomposites for structural applications

Saumy AGARWAL[1,*] and Satnam SINGH[1],

[1] *Department of Mechanical Engineering, National Institute of Technology Kurukshetra, Haryana, India*

***Corresponding author e-mail**: saumy_61900049@nitkkr.ac.in

Received date:
2 May 2025
Revised date:
11 December 2025
Accepted date:
20 March 2026

Keywords:
Al5052 composites;
Stir casting;
Titanium diboride (TiB_2);
Zirconia (ZrO_2);
Mechanical properties

Abstract

This study investigates the fabrication and mechanical characterization of Al5052 composites reinforced with nanosized TiB_2 and ZrO_2 particles via stir casting. Al5052 was chosen for its high strength-to-weight ratio and corrosion resistance, making it suitable for marine and automotive applications. The addition of hard ceramic reinforcements aimed to enhance mechanical properties without severely affecting ductility. Composite samples were tested as per ASTM standards. SEM analysis confirmed sound metallurgical bonding and generally uniform particle distribution. Density tests showed slight differences between theoretical and experimental values, with porosity generally increasing with reinforcement addition, attributed to particle agglomeration at higher loadings. Mechanical testing revealed an 18% increase in ultimate tensile strength for the hybrid composite with 1% TiB_2 and 1.5% ZrO_2. However, higher ZrO_2 content reduced ductility. Hardness improved significantly, with up to a 42% increase with ZrO_2 over the base alloy. Impact strength rose by over 69% with TiB_2 but declined at high ZrO_2 levels due to brittleness; hybrid composites showed moderate performance. Overall, the integration of nano-TiB_2 and nano-ZrO_2 into Al5052 enhanced strength and hardness, indicating strong potential for lightweight, high-performance applications in structural engineering, particularly in marine and automotive fields.

1. Introduction

In contemporary engineering applications, there is a growing demand for lighter equipment and machinery. However, modern materials are exposed to increasingly complex loading conditions and aggressive environmental conditions, rendering conventional monolithic materials inadequate for such demanding scenarios. To address such working conditions while meeting the demand for reduced weight, Metal Matrix Composites (MMCs) have emerged as a suitable class of materials. MMCs represent an advanced class of engineered materials combining two or more constituents to achieve superior mechanical and tribological properties. Emerged in the 1960s, these composites strategically integrate a metal matrix with reinforcement materials like particles of ceramics or fibers of organic materials to enhance structural characteristics [1]. The unique ability to transfer loads between matrix and reinforcement materials enables MMCs to mitigate the limitations of traditional monolithic materials, making them a critical innovation in contemporary materials engineering. While the reinforcing material can be made of metals or non-metals like ceramics (alumina, zirconia, titanium carbide, silicon carbide, titanium diboride, etc.) and organic materials (flyash, red mud, carbon fibres, etc.), the most commonly used matrix materials in the manufacturing of MMCs are aluminium, copper, magnesium, and titanium [2,3,4]. Amongst these different MMCs, Aluminium-based matrix composites (AMCs) have gained particular prominence due to their exceptional properties, including high specific strength, low thermal expansion, excellent wear resistance, and improved elevated temperature performance. By carefully selecting reinforcement materials and adjusting their composition, AMCs can be tailored to meet specific application requirements [5]. Due to cost restrictions, MMCs find their usage mainly in structural and engineering related industries such as automobile industry, aerospace industry, ship-building industry, and sports industry where the product requires good strength with minimal density or weight. Pistons, piston rings, disc brakes, cylinder linings, connecting rod etc. in automobiles are now being manufactured using AMCs [6,7]. These composites find their uses in bicycle frames, tennis rackets and other sport equipment. Railway carriages, bodies of ships and boats, helmets and ballistic armours, etc. are also made using hybrid-AMCs [8]. Interestingly, increasing the concentration of reinforcing particles can lead to reduced ductility in MMCs [9]. In contrast, incorporating very small amounts of nanoparticles can improve yield and tensile strength without significantly compromising ductility. Consequently, the development of nano-reinforced hybrid AMCs has gained momentum as a promising approach to further optimize the mechanical properties of these advanced composite materials [10,11].

This study examines Al5052 alloy as a matrix material for composite development. Al5052 is an aluminium-magnesium alloy, distinguished by its high strength-to-weight ratio and exceptional corrosion resistance. These attributes render it particularly suitable for demanding applications in aerospace, automotive, and marine industries. Common industrial applications of Al5052 include aircraft fuel and oil lines, fuel tanks, and various structural and transportation components, where lightweight durability and environmental resilience are critical design considerations

[12,13]. Despite these advantages, Al5052 remains limited by its non-heat-treatable nature, which restricts strengthening to cold working and results in only moderate tensile strength and hardness [14]. As a result, its applicability in high-load structural components like piston rings, engine liners, and brake pads is constrained. Enhancing its mechanical behaviour through ceramic nano-reinforcement is therefore both technically desirable and industrially relevant. Nano-scale reinforcements can overcome these limitations by promoting Orowan strengthening, grain refinement, and more effective load transfer, leading to improvements in strength and hardness [15]. However, incorporating nanoparticles into aluminium matrix introduces challenges such as poor wettability, particle agglomeration, sedimentation, and porosity formation during stir casting, all of which can weaken interfacial bonding and reduce reinforcement efficiency. Thus, Al5052 is selected as the matrix alloy with the aim of improving its mechanical properties while seeking to retain its inherent advantages, which are critical for its intended applications.

Yuan *et al*. [16] successfully fabricated Al5052 composites reinforced with $Al_{0.6}CoCrFeNi$ high entropy alloy (HEA) particles using vacuum hot-pressing sintering. Heat treatment significantly influenced interfacial characteristics and mechanical properties. A core-shell structure formed at the interface after 500°C heat treatment, with interfacial layer thickness increasing at higher temperatures and longer durations. This led to improved hardness (from 1.43 GPa to 1.81 GPa) and Young's modulus (from 77 GPa to 80 GPa). Nano-indentation tests confirmed that heat treatment enhanced micro-mechanical properties due to stress concentration and stronger interfacial bonding. The mechanical properties of Al 5052-based composites reinforced with boron carbide (B_4C) and graphite were examined by Kiran *et al.* [17]. The aluminium matrix composite specimens were produced by stirring 2%, 4%, 6%, and 8% boron carbide and graphite. SEM examination of the composite specimens indicated a somewhat homogeneous dispersion of B_4C and graphite particles throughout the matrix. The tensile strength increased to 186 MPa, which is about 21% more than the base alloy. Adding B_4C led to a modest increase in tensile strength. Adding 6% B_4C and 4% graphite to Al5052 resulted in increased tensile strength and improved mechanical characteristics. When compared to the base alloy, the composites' hardness increased by 19%. The composites exhibited a 19% enhancement in hardness relative to the base metal. Moreover, a heightened concentration of B_4C augmented the probability of brittle fracture.

Mohan *et al.* [18] examined the effect of silicon carbide (SiC) particles on the mechanical properties of stir-cast Al5052 alloy MMCs for rotor blade applications. SiC was added in varying compositions (2 wt% to 8 wt%), and the resulting composites underwent mechanical testing and microstructural analysis. SiC particles significantly enhanced tensile strength, with a 2% addition demonstrating an initial improvement. With improved dislocation density and stress dispersion, strength rose even further at 4% and 6% SiC. Better particle dispersion enhanced load transfer at 4% and 6% SiC, greatly increasing hardness. At 8% SiC produced the highest hardness and tensile strength, but too much SiC caused particle clustering and stress concentrations. The discrepancy between theoretical and actual densities suggested the presence of porosity or voids. Kukanur *et al*. [19] stir-casted the Al5052 based AMCs with B_4C particles as reinforcement with average size of 80 μm to 90 μm. B_4C particles were uniformly distributed throughout matrix, revealed from SEM analysis, which also demonstrated the good interfacial interaction of B_4C particles with the matrix. The inclusion of B_4C markedly improved the alloy's mechanical properties. The addition of 8 wt% B_4C enhanced the hardness of the Al5052 alloy composite by 30.23%, while ultimate and yield strengths increased by 24.2% and 29.1%, respectively. Despite these improvements, the addition of 8 wt% B_4C adversely affected ductility, as evidenced by a reduction in elongation from 14.8% to 11.3%. Fractographic analysis revealed a ductile fracture mode in the unreinforced alloy, while the composite exhibited a mixed brittle-ductile fracture mechanism.

Venkat *et al.* [20] fabricated Al5052-based composites via stir casting with 3 wt% Si_3N_4 and varying Al_2O_3 contents (2 wt% to 6 wt%). The composite with 2 wt% Al_2O_3 and 3 wt% Si_3N_4 exhibited the highest ultimate tensile strength (UTS) of 170.15 MPa. Variations in elongation at break were observed among the composites, with minimum and maximum values of 28.3% and 38.9%, respectively. Al_2O_3 and Si_3N_4 particles were uniformly disseminated within the Al5052 matrix, with little particle agglomeration. This uniform dissemination suggests strong interfacial bonding between the matrix alloy and the reinforcing particles.

Titanium diboride (TiB_2) offers high hardness, strength, and wear resistance, making it ideal for aerospace, automotive, and cutting tool applications. It exhibits excellent thermal stability, electrical conductivity, and corrosion resistance while maintaining a low density (approx. 4.52 $g \cdot cm^{-3}$). Additionally, TiB_2 enhances fracture toughness and is compatible with various metal matrices, improving overall mechanical performance [21]. In contrast, Zirconia (ZrO_2) provides remarkable wear resistance and thermal stability. Its chemical stability, abrasion resistance, and steel-like thermal expansion make it ideal for structural applications [22]. However, while ZrO_2 offers high inherent hardness, it is prone to agglomeration and localized stress concentrations that can significantly impair ductility and toughness when used in monolithic composites.

This study employs nanosized TiB_2 and ZrO_2 as hybrid reinforcements for Al5052 to exploit their complementary effects. Despite both ceramics exhibiting significant intrinsic hardness and strength, their effects on the aluminium matrix are distinct and dictated by their dispersion attributes and strengthening methods. TiB_2 is renowned for its exceptional intrinsic hardness and elastic modulus [23]. However, it is difficult to incorporate tiny TiB_2 particles into ex-situ casting processes due to wettability and agglomeration concerns, which can cause clustering and reduce the achievable hardening effect. When properly integrated, TiB_2 can enhance fracture toughness by promoting crack deflection and refining the matrix grains. Conversely, ZrO_2 is known for its remarkable ability to transfer interfacial loads, promoting dislocation hindrance and enhancing macroscopic hardness and tensile strength [24]. Nonetheless, ZrO_2 is susceptible to agglomeration at higher weight fractions, potentially resulting in micro-voids and brittle zones that can significantly diminish ductility and impact resistance. It is hypothesized that integrating these reinforcements in regulated ratios will mitigate the deficiencies inherent to each separate phase. Integrating the superior strengthening efficiency of the rigid ZrO_2 phase with the grain-refining properties of TiB_2 enables the optimization of the composite's micro-structural integrity. Theoretically, TiB_2 particles serve as physical barriers that disrupt the creation of extensive ZrO_2-rich agglomerated regions, thereby diminishing heterogeneity. Moreover, the density disparity

between the two phases is expected to hinder clustering, potentially reducing porosity and obstructing the development of brittle regions. Thus, ZrO_2 is anticipated to enhance stiffness and thermal stability, further improving the load-bearing capacity of TiB_2 without significantly undermining the integrity of the matrix. Consequently, employing a TiB_2-ZrO_2 hybrid approach for the Al5052 alloy presents a promising method to attain synergistic enhancements in total mechanical performance that neither reinforcement is likely to achieve independently. Such hybrids are well suited for structural components in automotive and marine applications where strength, wear resistance, and impact tolerance are critical. While monolithic composites have been studied, there is a significant lack of systematic characterization on the synergistic effects, microstructure control, and resultant mechanical performance of the Al5052-TiB_2/ZrO_2 hybrid system, especially concerning the optimization of the mixing ratio. This unexplored hybrid system (Al5052/ TiB_2/ZrO_2) therefore represents the primary research gap addressed in this work.

2. Materials and methods

2.1 Matrix and reinforcement

The matrix material utilized in this study was Al5052 alloy, selected for its superior strength-to-weight ratio, excellent formability, and weldability. Spectro analysis of Al5052 was done at CITCO-IDFC Testing Laboratory, Chandigarh. The chemical composition of Al5052 alloy, which includes magnesium, chromium, iron, silicon, zinc, and copper, is presented in Table 1. ZrO_2 nanoparticles were sourced from Nano Research Lab, Jamshedpur, while TiB_2 nanoparticles were obtained from Intelligent Materials Pvt. Ltd., Punjab. The key properties (as provided by the suppliers) of the materials are mentioned in Table 2.

2.2 Composite fabrication

The composite samples were produced using stir casting route as illustrated through a flow diagram shown in the Figure 1(a). It is a commonly utilised, adaptable, and economical technique for producing MMCs, which entails the mechanical agitation of solid ceramic particles into liquid metal, succeeded by solidification.

TiB_2 and ZrO_2 nanoparticles in an aluminium foil were preheated in a muffle furnace at 350°C for 1 h, promoting the elimination of moisture and gases from the nanoparticles while also diminishing the temperature gradient. Concurrently, approximately 800 g of Al5052 alloy were placed into a furnace heated to 700°C, where the alloy melted completely. Once the metal was thoroughly liquefied in the crucible, the preheated TiB_2 and ZrO_2 nanoparticles were carefully added. To enhance wettability, 0.5 wt% K_2TiF_6 powder and 0.5 wt% Mg were incorporated. To ensure uniform distribution of the ceramic nanoparticles within the molten base alloy, a mechanical stirrer equipped with high-strength steel impellers was used to agitate the mixture for 10 min in the furnace at a constant 350 rpm. After stirring, the composite slurry was held at 650°C for 60 s in a graphite crucible under static conditions inside the furnace. Vacuum pumping was done to prevent any gas or air entrapment [25]. Subsequently, the composite melt was poured into a preheated steel mould, where it was allowed to solidify. The mould used for casting contained three cavities: a 12 mm × 12 mm square section, a 20 mm diameter cylinder, and a 28 mm diameter cylinder, each with a length of 300 mm. For microstructural and mechanical testing, the cast bars were sectioned, and three specimens per composition were extracted from the central portion to ensure consistency and reliability. The schematic representation of the stir casting process is depicted in Figure 1(b). The composition of the test samples made for the study is presented in Table 3.

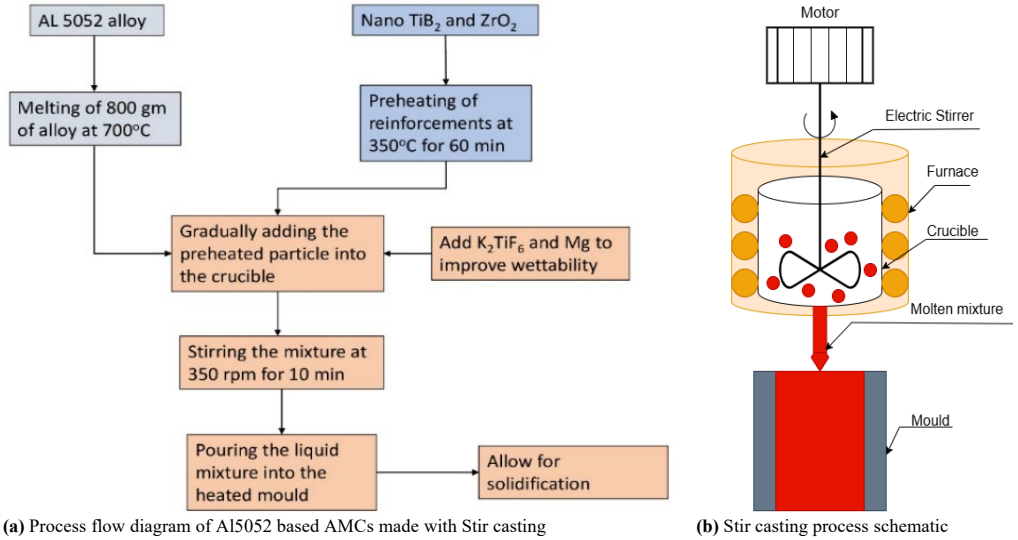

(a) Process flow diagram of Al5052 based AMCs made with Stir casting **(b)** Stir casting process schematic

Figure 1. Process flow and schematic of stir casting for Al5052-based AMCs.

Table 1. Chemical composition (weight %) of Al5052.

Elements	Si	Fe	Cu	Mn	Mg	Cr	Zn	Al
Composition	0.122	0.230	0.024	0.071	2.233	0.154	0.072	Balance

Table 2. Material properties.

Material	Purity	Average particle size (APS)	Density [gm·cc^{-1}]	Melting point [°C]
Al5052	Commercially available	-	2.70	605
TiB_2	99.9%	80 nm	4.52	3230
ZrO_2	99.9%	30-50 nm	5.89	2715

Table 3. Composition of Al5052-based Composite samples.

S. no.	Specimen no.	Composition		
		Al5052%	TiB_2%	ZrO_2%
1	B	100	0	0
2	S1	99	1	0
3	S2	98	2	0
4	S3	99	0	1
5	S4	98	0	2
6	H1	98.5	0.5	1
7	H2	98	1	1
8	H3	97.5	1	1.5

3. Experimental investigations

3.1 Characterization investigation

Scanning electron microscopy (SEM) was initially employed to examine the material's microstructure. To authenticate the elemental composition of powders and composites, an Energy-Dispersive Spectroscopy (EDS) analysis was also performed. Prior to characterization, the sample surfaces underwent meticulous polishing using a series of progressively finer emery sheets, ranging from 200 grit to 1200 grit. This comprehensive microstructural analysis facilitated the identification of phase distribution, phase morphology, and the spatial dispersion of reinforcement particulates within the matrix, thereby providing critical insights into the composite's structural integrity and material homogeneity. SEM and EDS tests were performed at NIT Kurukshetra and IIT Roorkee.

3.2 Density measurement

The density of MMCs is a critical parameter that affects their mechanical performance and overall suitability for various applications. Measuring the density helps evaluate material integrity, porosity levels, and the effectiveness of the reinforcement distribution within the matrix. The theoretical density (ρ_{th}) of an MMC is determined using the rule of mixtures. The experimental density (ρ_{exp}) of the composite is measured using the Archimedes method (average of 3 readings), which is based on fluid displacement [26].

$$\rho_{\text{exp}} = \frac{w_{\text{air}}}{w_{\text{air}} - w_{\text{water}}} \times \rho_{\text{water}}$$

Where w_{air} is the weight of composite in the air, w_{water} is its weight when submerged in distilled water, and ρ_{water} is the density of water at 20°C, which is 0.998 g·m^{-3}.

3.3 Tensile test

Using the wire electric discharge machining method, tensile specimens were painstakingly manufactured in accordance with the dimensional and geometric specifications that were outlined in the ASTM E8/E8M. This process ensures minimal thermal distortion and high dimensional accuracy, which is crucial for maintaining the integrity of the specimens. The dimensions of flat bar tensile specimens are 25 mm gauge length and 6 mm width (refer to Figure 2).

Following specimen preparation, they were subjected to tensile testing using a Universal Testing Machine (UTM). The testing was conducted at a controlled crosshead speed of 0.5 mm·min^{-1}. The application of a slow and uniform loading rate mitigated inertial effects, enabling precise evaluation of tensile properties. Each test was conducted on three specimens per composition, and the results are presented as mean values with standard deviations to ensure statistical reliability. The test yielded critical mechanical parameters, including ultimate tensile strength (UTS) and percentage elongation, which provide insights into the material's deformation behaviour and fracture resistance.

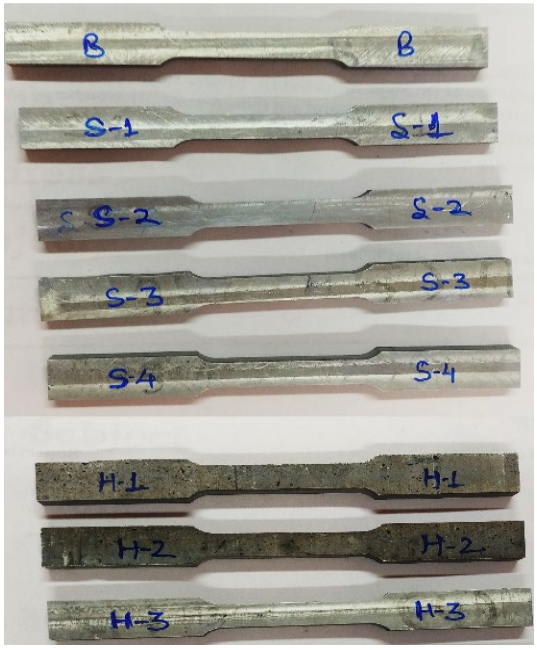

Figure 2. Tensile specimens of Al5052 based composites.

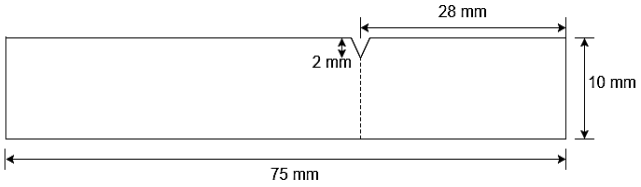

Figure 3. Schematic of an Izod test sample.

3.4 Hardness test

Vickers micro-hardness tests were performed as per ASTM E92 on polished sample surfaces using a 200 g load and a 15 s dwell duration. To obtain statistically reliable data, five randomly selected indentations were performed on each specimen, and the resulting hardness values were averaged to minimize variability and enhance measurement accuracy.

3.5 Impact test

The Izod impact test was performed according to ASTM E23-07 to determine the impact resistance of the composites. This test entails subjecting a notched specimen to a high-velocity pendulum strike, measuring the energy absorbed during fracture propagation. Impact tests were performed in triplicate for each composition, and the results are reported as mean values with standard deviations. The standardized notched specimens were prepared with dimensions of 75 mm × 10 mm × 10 mm, as shown in Figure 3.

4. Results and discussions

4.1 Characterization

SEM micrographs and EDS spectra of the reinforcement particles are shown in Figure 4. Figure 4(a-b) show the SEM micrographs of the as-received TiB_2 and ZrO_2 nanoparticles, confirming their irregular morphology and fine size. EDS mappings of TiB_2 and ZrO_2 nano-powders are presented in Figure 4(c-d), respectively. The detection of Ti and B peaks confirms the presence of TiB_2 particles, while the Zr and O peaks confirm the incorporation of ZrO_2. The EDS does not show unexpected or contaminant peaks, suggesting chemical purity of the reinforcements and good control during fabrication.

Figure 5 presents the SEM micrographs of the base alloy and the developed AMCs. Figure 5(a) depicts the microstructure of cast Al5052 alloy, which shows a relatively smooth surface without any reinforcement phase. In sample S1 (Figure 5(b)), TiB_2 nanoparticles show a fairly uniform distribution within the matrix, although isolated micro-crevices are visible. These minor defects may be linked to localized shrinkage during solidification and thermal expansion mismatch between the matrix and TiB_2. In sample S2 (Figure 5(c)), TiB_2 particles are incorporated into the matrix with some localized agglomeration, a result of the high surface energy of nanoparticles that promotes clustering. Sample S3 (Figure 5(d)) exhibits a more uniform dispersion of ZrO_2 nanoparticles with comparatively improved surface finish when compared with S1 and S2. This uniformity is attributed to the effective action of the wetting agent, which aided stabilized particle suspension during casting. In sample S4 (Figure 5(e)), ZrO_2 reinforcements are visible but with noticeable clustering, attributed to the increased particle count and incomplete breakup of nanoparticle agglomerates during stirring. The hybrid composites also revealed characteristic features. In sample H2 (Figure 5(f-g), taken at 500x and 1000x magnifications, the reinforcement phases are well dispersed within the Al5052 matrix, though micro-porosity and occasional clustering were observed. Higher magnification further shows embedded TiB_2 and ZrO_2 particles along with evidence of particle pull-out, likely caused by interfacial debonding during metallographic polishing. In sample H3 (Figure 5h), reinforcement phases are clearly visible, with distinct agglomeration and particle pull-out at a few isolated sites, indicating weaker interfacial bonding in those specific regions; however, the broader microstructure exhibits a fairly homogeneous dispersion of particles.

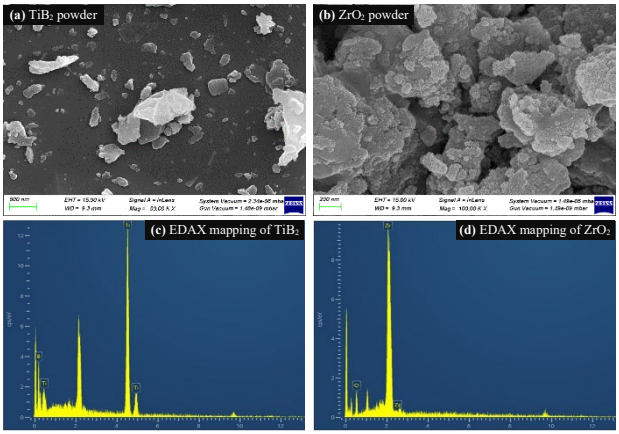

Figure 4. SEM and EDS of as-received TiB_2 and ZrO_2 powders.

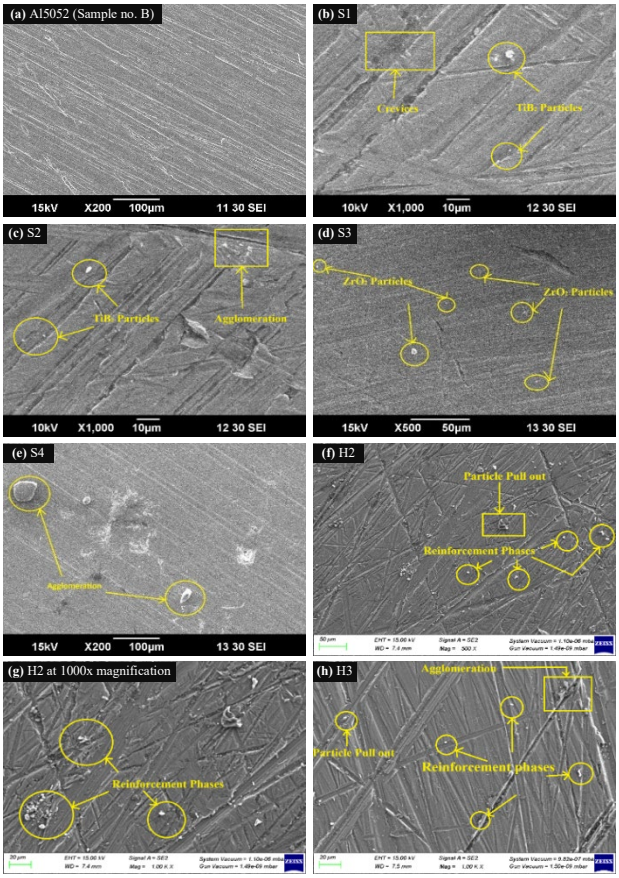

Figure 5. SEM of composite samples.

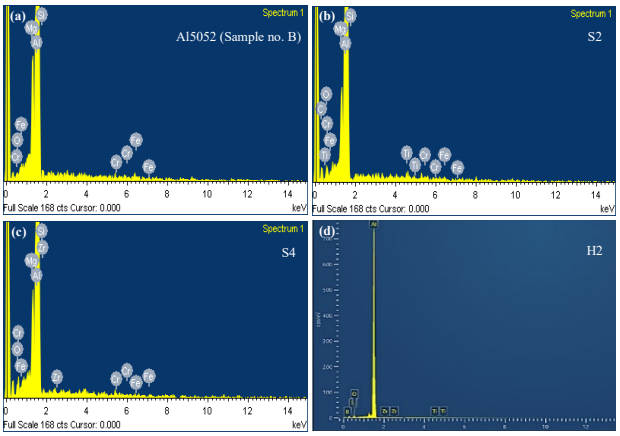

Figure 6. EDS of samples.

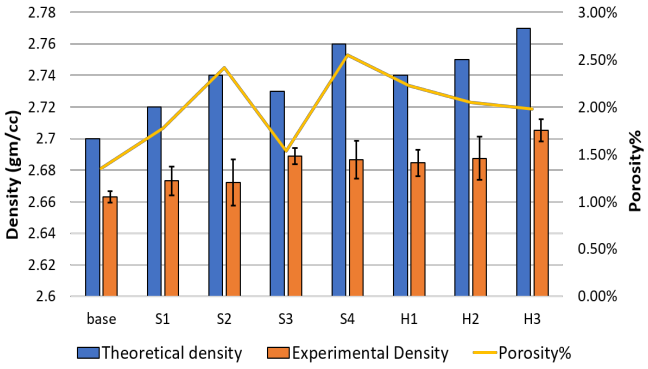

Figure 7. Density and Porosity of Al5052-based composites

Wetting was facilitated by preheating the TiB_2 and ZrO_2 powders, intentional addition of Mg (0.5 wt%) and K_2TiF_6 (0.5 wt%) as wetting agents, and stirring the melt at 350 rpm for 10 min. Mg additions are known to decrease contact angle in Al-ceramic systems by reducing the native oxide and lowering melt surface tension, while K_2TiF_6 functions as a flux or activator in Al melts that removes oxides and provides interfacial Ti, thereby enhancing particle wetting and dispersion [21]. These steps enabled effective reinforcement of the Al5052 matrix, although challenges regarding agglomeration and micro-porosity persisted. Combined with SEM and EDS evidence of Ti, B, Zr, and O distribution without agglomeration, these steps indicate adequate wettability in the composites. These observations confirmed that stir casting with wettability control enabled effective reinforcement of the Al5052 matrix, though agglomeration and particle pull-out remain challenges.

Results of EDS analysis of the samples are shown in Figure 6. EDS analysis of the base Al5052 alloy (Figure 6(a)) confirms the presence of aluminium (Al), magnesium (Mg), and silicon (Si) as primary constituents. EDS spectra for specimens S2 and S4, presented in Figure 6(b-c) respectively, further validate the successful incorporation of reinforcement elements. Specimen S2 revealed the presence of Al, Mg, Si, and titanium (Ti), along with trace elements such as chromium (Cr) and iron (Fe), likely originating from alloying elements or processing equipment. In contrast, specimen S4 displayed distinct peaks corresponding to zirconium (Zr), oxygen (O), silicon (Si), magnesium (Mg), and within the matrix. EDS of H2 (Figure 6(d)) chromium (Cr), corroborating the effective embedding of ZrO_2 particles) revealed the presence of Ti, Boride (B), Zr, O and Al constituents of sample. These results collectively demonstrate the compositional integrity and elemental distribution in the developed composites.

4.2 Density analysis

Figure 7 depicts the variation in densities and porosity of samples as a function of reinforcement concentration. It is evident that the experimentally measured densities are marginally lower than the corresponding theoretical values, primarily due to factors such as porosity and possible defects in the fabrication process [12,27]. The incorporation of TiB_2 and ZrO_2 reinforcements results in a general increase in both theoretical and experimental densities, reflecting the contribution of higher-density reinforcement phases to the composite matrix. However, the experimental results reveal subtle differences when examined in conjunction with the SEM observations. For instance, S1 (Al5052/1 wt% TiB_2) exhibits a slightly higher experimental density (2.6731 $g{\cdot}cm^{-3}$) compared to S2 (Al5052/2 wt% TiB_2), despite the latter containing a higher fraction of TiB_2. This reduction in effective density for S2 is consistent with the higher porosity observed in the SEM micrographs, where localized TiB_2 agglomeration promotes void entrapment during solidification and hinders densification. In contrast, S1 demonstrates a more homogeneous particle dispersion with minimal clustering, leading to reduced porosity and marginally higher effective density.

Furthermore, the Figure 7 reveals that hybrid composites also exhibit higher porosity compared to the base alloy. This increase in porosity can be attributed to factors such as inadequate mixing of the reinforcement particles within the matrix and variations in their wettability. Notably, specimen S4 (Al5052/2% ZrO_2) exhibits the highest porosity among all samples (2.55%). This indicates that increasing the ZrO_2 wt% to 2% exceeds a saturation threshold, leading to significant clustering that hinders matrix infiltration. In the case of hybrid composites, the trend reveals the efficacy of the hybrid reinforcement strategy. Contrary to the monolithic trends, H1 (0.5% TiB_2/1% ZrO_2) displayed the highest porosity (2.23%) among the hybrid specimens. This suggests that a critical threshold of TiB_2 particles is required to effectively break up ZrO_2 clusters. In H1, the TiB_2 content (0.5 wt%) was insufficient to facilitate this dispersion, leading to localized void formation. Conversely, H3 (1% TiB_2/1.5% ZrO_2) demonstrated a lower porosity (1.98%) despite having a higher total reinforcement fraction. This confirms that the presence of sufficient TiB_2 aids in the physical dispersion of ZrO_2, enhancing matrix infiltration and minimizing bulk porosity, resulting in a denser composite structure. Density analysis of Al5052-matrix composites was conducted by Mohan *et al.* [28], to study the effect of Silicon carbide (SiC) and alumina (Al_2O_3). Significant improvement of density was observed by both single-reinforced composites and hybrid composites.

4.3 Tensile test

Figure 8(a) illustrates the UTS of Al5052-based composites reinforced with varying concentrations of TiB_2 and ZrO_2. The base Al5052 alloy exhibits the lowest UTS at 148.3 MPa, which serves as a reference for assessing the influence of reinforcement addition.

A noticeable improvement in UTS is observed with the incorporation of reinforcements, suggesting effective stress transfer from the ductile matrix to the rigid particles. The addition of TiB_2 led to an increase in UTS, with 1% TiB_2 (S1) achieving 156.6 MPa and 2% TiB_2 (S2) reaching 159.1 MPa. This enhancement is likely attributed to the combined contribution of load-bearing and dislocation-based strengthening mechanisms. Owing to its high elastic modulus and hardness, TiB_2 effectively carried a portion of the applied load, thereby reducing the stress borne by the aluminium matrix. Simultaneously, the TiB_2 nanoparticles acted as obstacles to dislocation motion, promoting Hall-Petch strengthening through grain refinement [29]. However, the strengthening efficiency in S2 appeared partially limited, likely due to particle clustering which reduces the effective interfacial area available for stress transfer. Similarly, ZrO_2-reinforced composites showed an improvement in UTS, reaching 161.7 MPa (S3) and 168.2 MPa (S4). The rigid ZrO_2 particles presumably facilitated significant Orowan strengthening by impeding dislocation glide. Furthermore, the coefficient of thermal expansion (CTE) mismatch between ZrO_2 and the Al5052 matrix likely generated a high density of dislocations around the particles during cooling, thereby increasing resistance to plastic deformation.

The UTS of hybrid composites exhibits a synergistic trend. Sample H3 (Al5052/1% TiB_2/1.5% ZrO_2) achieved the maximum UTS of 175.5 MPa, followed by H2 (168.3 MPa). This superior strength is attributed to the complementary strengthening mechanisms of the hybrid reinforcements: TiB_2 primarily acts as a grain refiner (Hall-Petch strengthening), while the stiffer ZrO_2 particles bear the majority of the applied load (load transfer mechanism). Moreover, the reduced porosity in H2 and H3 (discussed in Section 4.2) suggests that TiB_2 aided in the physical de-agglomeration of ZrO_2 clusters, thereby enhancing dispersion and load transfer efficiency. In contrast, H1 (Al5052/0.5% TiB_2/1% ZrO_2) displayed the lowest UTS among the hybrid composites (155.5 MPa). This reduced strength in H1 is primarily attributed to the combination of lower reinforcement content and localized porosity. This observation correlates directly with the density trends observed in Figure 7. As shown in the porosity analysis, H1 exhibited a porosity of 2.23%, which is notably higher than the porosity levels observed in H2 (2.05%) and H3 (1.98%). This increased porosity reduces the effective cross-sectional area available to support the applied load. Unlike samples H2 and H3, where higher reinforcement fractions provided sufficient strengthening to overpower microstructural defects, the lower reinforcement content in H1 was insufficient to fully compensate for the weakening effects of this porosity. However, it is important to note that excessive reinforcement additions may cause particle agglomeration and increased porosity, potentially functioning as stress concentrators, thereby limiting further tensile strength enhancement [30-32]. Similar trends have been reported in literature; for instance, Kumar *et al.* [33] investigated the effect of Zirconium diboride (ZrB_2) on composites made with Al5052 matrix material. There was increase in UTS from 89 MPa for base alloy to the maximum UTS of 161 MPa for sample with 9% ZrB_2. Sharp decline in UTS was observed when the % ZrB_2 was further increased, as a result of agglomeration of particles.

Despite the enhancement in strength, reinforced samples exhibited a significant reduction in ductility, as illustrated in Figure 8(b). The base alloy exhibited the highest ductility, with a strain at peak stress of approximately 13.7% and a strain at break of 17.8%, whereas composites with higher reinforcement content experienced a drastic decline in ductility. This reduction can be attributed to several factors, including restricted plastic deformation due to the presence of hard ceramic particles, increased stress concentrations at particle-matrix interfaces, and potential particle agglomeration, which led to premature failure. At higher reinforcement contents, the reduction in ductility may also be associated with non-uniform particle dissemination. Particle clusters are expected to generate localized triaxial stress states that facilitate early void nucleation and coalescence under tensile loading, thereby limiting uniform plastic deformation. Consequently, these agglomerates likely acted as dominant stress concentrators, contributing to the sharp reduction in ductility and the saturation of strength at higher reinforcement levels [16].

Among the monolithic composites, TiB_2-reinforced samples showed a moderate reduction in ductility, while ZrO_2 reinforcements had an even more detrimental effect on ductility showing lower strain values. This drastic reduction is attributed to severe particle clustering and weaker interfacial bonding rather than intrinsic hardness alone. Furthermore, the higher porosity levels associated with certain ZrO_2 additions exacerbated this embrittlement by promoting void coalescence, which significantly increased localized stress concentrations and accelerated premature failure. However, the Hybrid composites (H1, H2, and H3) exhibit a unique advantage. Despite a progressive decline in ductility with increasing reinforcement content, they maintain superior strain values compared to their ZrO_2-only counterparts. H1 (7.11% strain at peak, 9.67% at break) surpasses S3 in ductility, indicating that the TiB_2-ZrO_2 synergy facilitates a more uniform stress distribution, mitigating ZrO_2-induced embrittlement. Similarly, H2 (6.14% strain at peak, 8.95% at break) and H3 (4.94% strain at peak, 6.88% at break) exhibit greater ductility than S4, suggesting that hybrid reinforcement optimizes stress transfer while reducing stress concentrations.

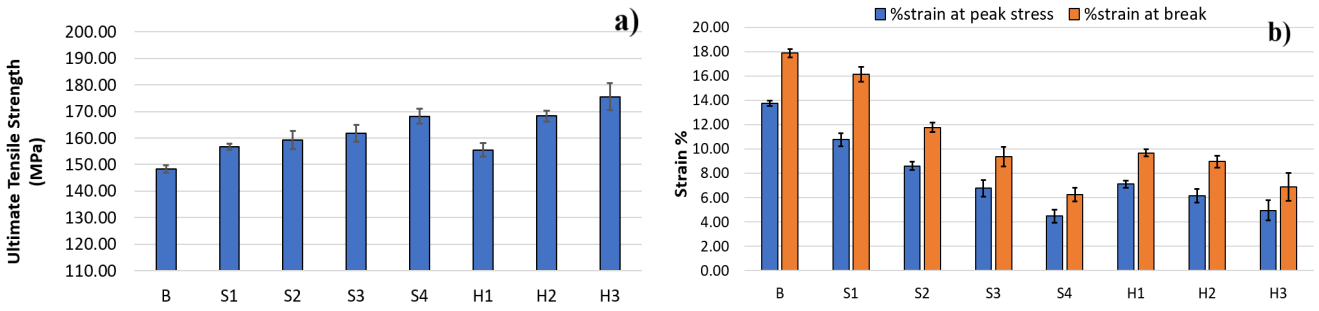

Figure 8. (a) UTS of Al5052-based AMCs and (b) Elongation% of Al5052-based AMCs.

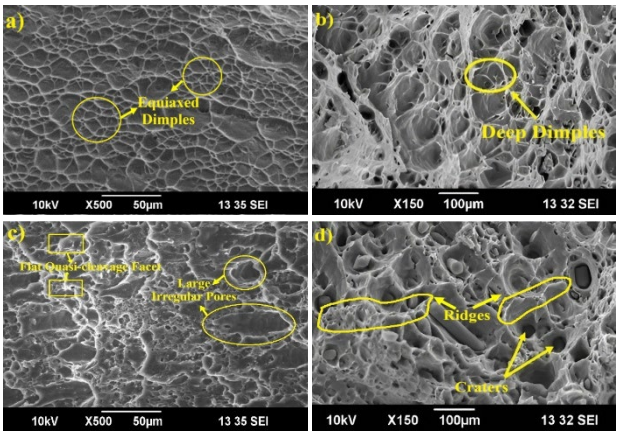

Figure 9. SEM of fractured surface of tensile specimen.

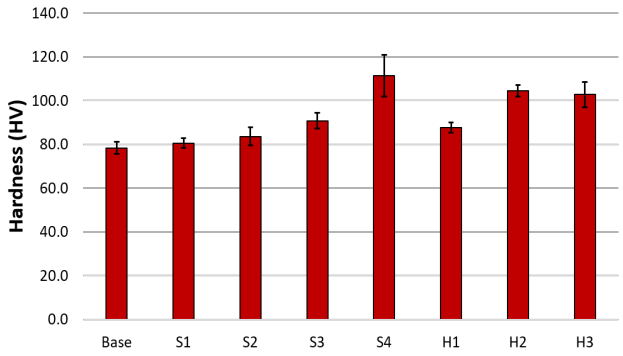

Figure 10. Vicker's Hardness results.

Notably, H3, despite a higher reinforcement fraction than S4, retains superior strain values, underscoring the efficacy of balanced hybridization in counteracting excessive brittleness. Furthermore, H2 and H3 outperform S2, S3, and S4 by achieving higher tensile strength while preserving a more favourable strength-ductility balance. It should be noted that the present investigation is limited to the as-cast condition in order to isolate and evaluate the effects of TiB_2 and ZrO_2 reinforcement on Al5052. Mechanical working of the cast bars, which could further refine the microstructure and enhance strength, was not undertaken as it lies outside the scope of this study. Ravikumar *et al.* [34] reported that the tensile strength of Al6082 composites increases steadily with tungsten carbide addition up to 8%, reaching approximately 188 MPa, while the base Al6082 alloy exhibited a tensile strength of about 162 MPa. Similarly, it has been reported [19] that the ultimate tensile strength (UTS) of stir-cast Al5052 alloy increased from 136.1 MPa (base alloy) to 155.8 MPa at 4 wt% B_4C and further to 179.6 MPa at 8 wt% B_4C, demonstrating a significant enhancement with increasing reinforcement content. In another study [20], the UTS of Al5052 composites reinforced with 3 wt% Si_3N_4 and varying Al_2O_3 content was measured as 170.15 MPa (2 wt% Al_2O_3), 134.47 MPa (4 wt% Al_2O_3), and 142.41 MPa (6 wt% Al_2O_3).

Figure 9(a-d) depicts the fractured surface of tensile samples. The unreinforced base alloy reveals a fracture surface (refer to Figure 9(a)) dominated by deep, equiaxed dimples, indicative of significant plastic deformation and a failure mechanism driven by micro-void coalescence. In S2 (2% TiB_2), the fracture mode remains predominantly ductile with visible matrix tearing and no evidence of brittle cleavage; however, the surface is characterized by deep, enlarged voids (refer to Figure 9(b)). These characteristics validate the void entrapment mechanism, wherein TiB_2 agglomerates impede liquid flow after solidification. Conversely, S4 (2% ZrO_2) exhibits a transition to brittle failure, featuring flat quasi-cleavage facets and large irregular pores that facilitated rapid crack propagation, aligning with its minimal strain values (refer to Figure 9(c)). The hybrid composite (H1) displays a mixed-mode fracture in which the matrix retains some ductility, while the surface is disrupted by distinct, localized craters (refer to Figure 9(d)). These defects correspond to the high porosity, where insufficient TiB_2 content failed to fully deagglomerate ZrO_2 clusters, creating localized sites for decohesion and void formation. The fine TiB_2 reinforcement allowed for some plastic stretching (ridges), but the failure was ultimately triggered by the stress concentration at the large processing defects (craters) caused by insufficient ZrO_2 dispersion.

4.4 Hardness test

The hardness values of Al5052-based composites, as illustrated in the Figure 10, demonstrate a notable improvement following reinforcement with TiB_2 and ZrO_2. The base Al5052 alloy has the lowest hardness (78.3 HV) and serves as a benchmark for comparison. Adding TiB_2 causes a slight increase in hardness in S1 sample (80.5 HV), which increases further to 83.6 HV by increasing TiB_2 content to 2% in S2 sample. This enhancement is largely ascribed to the Hall-Petch strengthening mechanism, where TiB_2 particles act as nucleating agents that refine the matrix grain size, thereby increasing the resistance to plastic deformation. In contrast, ZrO_2-reinforced composites showed a significant improvement in hardness, with S4 (Al5052/2% ZrO_2) having the maximum hardness of 111.3 HV. The superior hardness is attributed to the high rigidity of the ZrO_2 particulates. These hard particles serve as effective barriers to dislocation motion (Orowan strengthening). The significant disparity in the CTE between the Al matrix and ZrO_2 likely generated a high density of dislocations around the particles during solidification, thereby enhancing the matrix's hardness through strain hardening.

The hardness response of the present Al5052 composites corroborates prior findings on different aluminium alloys reinforced with TiB_2 and ZrO_2. Suresh and Moorthi [35] investigated Al6061 reinforced with TiB_2 and reported only a modest rise in hardness from 65.53 VHN for the base alloy to 70.26 VHN at 4 wt% TiB_2, indicating that ex-situ added TiB_2 particles contributed only limited strengthening (improvement in hardness by 7.21%). In contrast, Madhusudhan *et al.* [36] observed a much sharper increase in hardness for ZrO_2-reinforced AA7068, where the value rose from 93.5 VHN for the base alloy to 104.6 VHN at 4 wt% ZrO_2, corresponding to an 11.87% increase. Similarly, Nagasai *et al.* [37] reported Al6061-ZrO_2 composites fabricated by stir casting, with hardness values exceeding 110 VHN at approximately 3 wt% reinforcement.

The observed hardness behaviour is closely linked to the competition between the strengthening mechanisms and microstructural defects. Specimens reinforced with TiB_2 exhibited reduced experimental density and higher porosity, which impaired effective stress transfer across the interface and increased local compliance under indentation, thereby limiting the macroscopic hardness increment despite the superior intrinsic hardness of TiB_2. Despite the addition of K_2TiF_6

and Mg to improve wettability, ex-situ TiB_2 still exhibited clustering and porosity (2.41% for S2), which limited its effectiveness. Conversely, ZrO_2-reinforced specimens achieved the maximum hardness (111.3 HV for S4) despite exhibiting the highest porosity (2.55%). This indicates that the strengthening contributions of ZrO_2 (Orowan strengthening and CTE mismatch) were sufficiently dominant to overpower the softening effects of the void volume [2,3]. These results confirm that the hardening efficiency in the as-cast Al5052 system is dictated predominantly by the magnitude of the dislocation obstruction mechanisms and the quality of reinforcement dispersion, rather than by the intrinsic hardness of the ceramic reinforcement alone.

Hybrid composites (H1, H2, and H3) exhibited higher hardness values than the base alloy and monolithic TiB_2-reinforced samples, although somewhat lower than the highest hardness achieved by S4. H2 sample (104.4 HV) outperformed H1 (87.6 HV) and H3 sample (102.7 HV) in terms of hardness. However, the slight hardness decrease in H3 suggests that increasing ZrO_2 content beyond the optimal level induces minor localized clustering. Despite having the lowest bulk porosity (1.98%), H3 exhibited agglomeration and particle pull-outs at few isolated sites in SEM analysis. These localized inhomogeneities weaken interfacial bonding at specific sites, limiting the effective indentation resistance. The overall hardness enhancement in the hybrid samples is attributed to the synergistic effect of effective load transmission and Orowan strengthening by ZrO_2, alongside Hall-Petch strengthening resulting from matrix grain refinement by TiB_2 [13,38]. Crucially, while the monolithic S4 sample achieved the highest absolute hardness, this came at the cost of ductility due to severe particle segregation. The hybrid systems (H2, H3) successfully mitigated this trade-off, retaining high hardness while avoiding the severe embrittlement observed in high-fraction monolithic ZrO_2-composites (S4). Farooq *et al.* [39] manufactured Al5052-based AMCs with 0 wt% to 7.5 wt% of TiB_2 microparticles. The hardness was increased from 65.5 HV to 85.16 HV due grain refinement, dispersion strengthening, and interfacial bonding. Jacobdhas *et al*. [40] investigated the effect of adding Tungsten carbide (WC) and graphite on hardness of Al5052-based AMCs. It was observed that hardness value was increased by 10.3% due to high density of WC particles.

4.5 Impact test

The Izod impact test result, as shown in Figure 11, illustrates the influence of reinforcement composition on the impact strength of Al5052-based composites. The unreinforced alloy exhibited an impact energy of 6.20 J. It is observed that TiB_2 enhances toughness, with 1% and 2% TiB_2 achieving 7.8 J and 10.5 J, respectively. This improvement is attributed to the grain refinement effect (discussed in earlier sections) which creates a finer microstructure where the increased density of grain boundaries acts as an effective barrier to crack propagation [41]. Additionally, owing to the strong interfacial bonding, the well-dispersed TiB_2 particulates likely facilitated energy dissipation through crack deflection mechanisms. By forcing the crack front to meander around the rigid particles rather than causing particle pull-out, the reinforcement increases the total fracture surface area and the energy required for failure. In contrast, ZrO_2 reduces impact resistance, with 1% and 2% ZrO_2 recording 4.5 J and 3.9 J respectively, attributed to increased brittleness. Density data (Figure 7) clarifies this drop in toughness. Sample S3 exhibited low porosity yet poor toughness, indicating failure was driven by brittle clusters and interfacial decohesion rather than voids. In contrast, the further drop in S4 (3.9 J) resulted from combined clustering and the highest recorded porosity (2.55%), which significantly reduced the load-bearing cross-section. Hybrid composites exhibited intermediate toughness (5.6 J to 6.4 J), confirming that the presence of TiB_2 effectively interrupts the brittle regions formed by ZrO_2, thereby minimizing the large defect sites responsible for catastrophic failure and recovering the composite's impact tolerance.

Natarajan *et al.* [41] investigated the impact response of Friction stir processed hybrid AMCs reinforced with yttrium oxide (Y_2O_3) and SiC (1% to 3%). The inclusion of hard ceramic particles significantly enhances toughness, with Al-3SiC-1Y_2O_3 achieving a 75.96% improvement over the base Al5052 alloy, whereas Al-1SiC-3Y_2O_3 achieved only 32.1% improvement. Overall, optimal impact performance is achieved through the combined effects of grain refinement and balanced hybrid particle dispersion. Similar findings were made by Jacobdhas *et al.* [40] where impact strength of Al/WC/graphite composites exhibited a notable improvement of approximately 34.2% over the pure as-cast Al5052 alloy, highlighting the effectiveness of hybrid reinforcement in enhancing toughness. In comparison, reinforcement with SiC and graphite led to a lower impact strength enhancement of 21.88%, likely due to the formation of brittle intermetallic phases that compromise energy absorption capacity. Ravi Kumar *et al.* [42] investigated the addition of 2 wt% to 10 wt% TiC to Al 6063 alloy and reported a continuous decrease in impact strength, with a maximum reduction of approximately 32% at 10 wt% reinforcement. The decline in toughness was associated with the brittle nature of the ceramic phase, which restricted matrix plasticity and intensified stress concentrations. The presence of TiC facilitated microcrack initiation, accelerated crack propagation, and promoted interfacial debonding between the matrix and reinforcement, thereby reducing the material's capacity to absorb impact energy. In contrast, D.A. Tirfe *et al.* [43] examined Al6061 reinforced with bamboo leaf stem ash (BLSA) in the range of 2.5 wt% to 7.5 wt% and observed impact energy values between 8.24 J and 14.82 J. The optimum toughness was achieved at 5 wt% BLSA under moderate processing parameters, where uniform particle dispersion and strong interfacial bonding enhanced the energy absorption. At higher reinforcement levels, particle agglomeration and stress localization reduced the ability of the composite to dissipate deformation energy, resulting in lower impact resistance. With respect to hybrid composites, Venkat *et al.* [20] examined Al5052-based

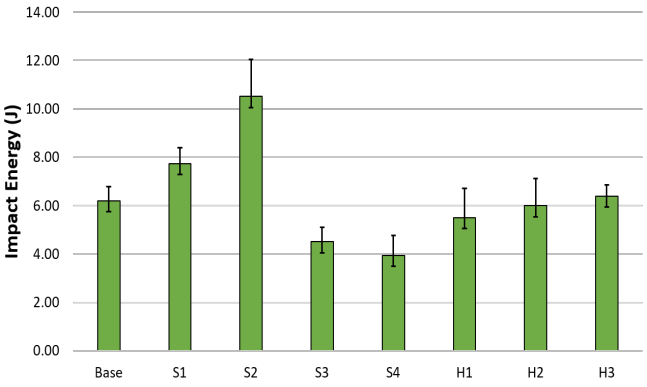

Figure 11. Izod Impact test result of Al5052 composite samples.

hybrid composites containing Al_2O_3 and Si_3N_4 and reported that these MMCs exhibited a marked improvement in impact toughness, reaching a peak of 12 J at moderate Al_2O_3 levels. This enhancement was attributed to uniform distribution of reinforcement and effective particle-matrix interactions, which facilitated better energy absorption under impact loading. However, when Al_2O_3 content was increased beyond the optimum (above 4%), the toughness declined to 10 J due to agglomeration and embrittlement, which promoted crack initiation and reduced ductility.

5. Conclusion

This study effectively synthesized Al5052-based AMCs reinforced with nano-TiB_2 and nano-ZrO_2 by stir casting, followed by an analysis of their mechanical and physical properties. Following conclusions are made:

SEM micrographs show generally uniform particle distribution at low reinforcement levels, while higher loadings in monolithic composites (S2 and S4) led to particle agglomeration and localized porosity. However, hybrid composites (H2 and H3) exhibited improved particle dispersion, confirming the effectiveness of the hybrid reinforcement strategy.

The density increased with reinforcement content due to the higher density of TiB_2 and ZrO_2. However, porosity also rose, especially in hybrid composites, with H1 and S4 exhibiting the highest porosity due to agglomeration and poor wettability.

The addition of reinforcements improved UTS by up to 18% (in H3) due to effective dislocation impediment and load transfer, although this came at the cost of reduced ductility as the hard ceramic phases restricted matrix deformation. Hybrid composites (H1, H2, H3) retained better strain values than ZrO_2-only composites due to improved stress distribution.

Hardness increased with reinforcement, peaking at 111.3 HV in S4. Hybrid composites also showed notable improvement, with H2 and H3 reaching 104.4 HV and 102.7 HV respectively, owing to combined effects of load transfer and dislocation obstruction.

TiB_2 improved toughness (up to 10.5 J), while ZrO_2 decreased it (down to 3.9 J). Hybrid composites balanced the trade-off, achieving intermediate values (5.6 J to 6.4 J), mitigating ZrO_2-induced brittleness through TiB_2's toughening effect.

This study demonstrates that hybridizing nano-TiB_2 and nano-ZrO_2 provides a synergistic effect, where TiB_2's toughening and grain-refining properties help mitigate the embrittlement caused by the hard and strengthening ZrO_2 phase, leading to a superior balance of strength and toughness not achievable with monolithic reinforcement. Consequently, H2 and H3 are identified as optimal composites for structural applications such as fuel tank, cylinder liners, brake pads, and piston rings.

While this study demonstrates the synergistic potential of Al5052-TiB_2/ZrO_2 hybrid composites, certain limitations like porosity and agglomeration during casting were observed. Future work will focus on optimizing process parameters to produce defect-free composites with improved dispersion. The impact of secondary processing, such as mechanical working, may be explored in the future. Furthermore, assessing electrochemical corrosion resistance will be essential to validate these hybrids for next-generation maritime applications.

Acknowledgements

The authors gratefully acknowledge NIT Kurukshetra for providing necessary facilities and support for this research.

References

[1] S. Agarwal, S. Angra, and S. Singh, "A review on the mechanical behaviour of aluminium matrix composites under high strain rate loading," *Materials Physics and Mechanics*, vol. 51, no. 6, pp. 1–13, 2023.

[2] S. Agarwal, and S. Singh, "Production techniques and properties of particulate reinforce metal matrix composites: A review," *Materials Physics and Mechanics*, vol. 52, no. 6, pp. 136–153, 2024.

[3] V. Chak, H. Chattopadhyay, and T. L. Dora, "A review on fabrication methods, reinforcements and mechanical properties of aluminum matrix composites," *Journal of Manufacturing Processes*, vol. 56, pp. 1059–1074, 2020.

[4] D. Kumar, S. Angra, and S. Singh, "Mechanical properties and wear behaviour of stir cast aluminum metal matrix composite: A review," *International Journal of Engineering, Transactions A: Basics*, vol. 35, no. 4, pp. 794–801, 2022.

[5] R. Pandiyarajan, P. Maran, S. Marimuthu, and M. P. Prabakaran, "Investigation on mechanical properties of ZrO_2, C and AA6061 metal matrix composites," *Advances in Materials and Processing Technologies*, vol. 00, no. 00, pp. 1–9, 2020.

[6] D. B. Miracle, "Metal matrix composites - From science to technological significance," *Composites Science and Technology*, vol. 65, no. 15-16, pp. 2526–2540, 2005.

[7] J. Kumaraswamy, K. C. Anil, T. R. Veena, G. Purushotham, and K. S. Kumar, "Investigating the mechanical properties of Al 7075 alloy for automotive applications: synthesis and analysis," *Evergreen*, vol. 10, no. 3, pp. 1286–1295, 2023.

[8] J. Suthar, and K. M. Patel, "Processing issues, machining, and applications of aluminum metal matrix composites," *Materials and Manufacturing Processes*, vol. 33, no. 5, pp. 499–527, 2018.

[9] M. Y. Khalid, R. Umer, and K. A. Khan, "Review of recent trends and developments in aluminium 7075 alloy and its metal matrix composites (MMCs) for aircraft applications," *Results in Engineering*, vol. 20, 2023.

[10] R. Casati, and M. Vedani, "Metal matrix composites reinforced by nano-particles—A review," *Metals*, vol. 4, no. 1, pp. 65–83, 2014.

[11] A. V. Muley, S. Aravindan, and I. P. Singh, "Nano and hybrid aluminum based metal matrix composites: An overview," *Manufacturing Review*, vol. 2, 2015.

[12] M. Patel, S. K. Sahu, and M. K. Singh, "Fabrication and investigation of mechanical properties of SiC particulate reinforced AA5052 metal matrix composite," *Journal of Modern Materials*, vol. 7, no. 7, pp. 26–36, 2020.

[13] A. Dolatkhah, P. Golbabaei, M. K. Besharati Givi, and F. Molaiekiya, "Investigating effects of process parameters on

microstructural and mechanical properties of Al5052/SiC metal matrix composite fabricated via friction stir processing," *Materials and Design*, vol. 37, pp. 458–464, 2012.

[14] J. R. Davis, "Aluminum and aluminum alloys," in *Alloying: Understanding the Basics*, ASM International, pp. 351–416. 2001.

[15] Z. Zhang, and D. L. Chen, "Consideration of Orowan strengthening effect in particulate-reinforced metal matrix nanocomposites : A model for predicting their yield strength," *Scripta Materialia*, vol. 54, no. 7, pp. 1321–1326, 2006.

[16] Z. Yuan, W. Tian, F. Li, Q. Fu, X. Wang, W. Qian, and W. An, "Effect of heat treatment on the interface of high-entropy alloy particles reinforced aluminum matrix composites," *Journal of Alloys and Compounds*, vol. 822, p. 153658, 2020.

[17] K. Kiran, K. Ravikumar, and V. S. S. Balaji, "Materials today: Proceedings effect of B_4C and graphite particulates on the mechanical and micro structural characteristics of AA 5052 hybrid composites," *Materials Today: Proceedings*, vol. 27, no. 3, pp. 2935–2940, 2020.

[18] V. Mohan, N. B. Doddapattar, and K. S. Kumar, "Effect of silicon carbide particulates on mechanical behavior of Al5052 alloy metal matrix composites for mining applications," *Journal of Mines, Metals and Fuels*, vol. 72, no. 8, pp. 893–904, 2024.

[19] V. Kukanur, K. C. Vishwanath, N. Namdev, T. H. Manjunatha, B. Valukula, and S. M. Kumar, "Investigations on hardness and tensile behavior of micron boron carbide particles reinforced Al5052 alloy composites," *Brazilian Journal of Development*, vol. 11, no. 2, p. e77757, 2025.

[20] P. Pavan Venkat, P. Chinnam Naidu, L. Y. N. Pavan Kumar, K. Vivek Babu, M. Krishna Prasad, and M. Venkateswara Rao, "Effect of Al_2O_3 particles on mechanical, microstructural and tribological characteristics of Al5052 metal matrix composite reinforced with Si_3N_4 particles," *Materials Today: Proceedings*, vol. 91, pp. 158–166, 2023.

[21] Y. Pazhouhanfar, and B. Eghbali, "Microstructural characterization and mechanical properties of TiB_2 reinforced Al6061 matrix composites produced using stir casting process," *Materials Science and Engineering A*, vol. 710, pp. 172–180, 2018.

[22] R. Shetty, P. R. Gurupur, J. Hindi, A. Hegde, N. Naik, M. S. S. Ali, I. S. Patil, and M. Nayak, "Processing, mechanical characterization, and electric discharge machining of stir cast and spray forming-based Al-Si alloy reinforced with ZrO_2 particulate composites," *Journal of Composites Science*, vol. 6, no. 11, p. 323, 2022.

[23] B. Basu, G. B. Raju, and A. K. Suri, "Processing and properties of monolithic TiB_2 based materials," *International Materials Reviews*, vol. 51, no. 6, pp. 352–374, 2006.

[24] S. Roseline, V. Paramasivam, and S. Jayabal, "Evaluation of structure and mechanical properties of zirconia reinforced aluminium matrix composites," *Journal of Computational and Theoretical Nanoscience*, vol. 15, no. 3, pp. 830–838, 2018.

[25] M. C. Gui, J. M. Han, and P. Y. Li, "Microstructure and mechanical properties of Mg-Al_9Zn/SiCp composite produced by vacuum stir casting process," *Materials Science and Technology*, vol. 20, no. 6, pp. 765–771, 2004.

[26] N. Faisal, and K. Kumar, "Mechanical and tribological behaviour of nano scaled silicon carbide reinforced aluminium composites," *Journal of Experimental Nanoscience*, vol. 13, pp. S1–S13, 2018.

[27] M. Nagaral, P. K. Raghavendra, V. Auradi, V. Bharath, S. Patil, and M. S. Tattimani, "Effect of micro raphite particles on the microstructure and mechanical behavior of aluminium 6061 (Al-Mg-Si) alloy composites developed by novel two step casting technique," *Journal of Metals, Materials and Minerals*, vol. 31, no. 2, pp. 38–45, 2021.

[28] V. Mohan, N. B. Doddapattar, Mallaradhya H. M., and S. Deshpande, "Characterization of Al5052 based metal matrix composites reinforced with SiC and Al_2O_3," *Tuijin Jishu/ Journal of Propulsion Technology*, vol. 44, no. 4, pp. 5398–5406, 2023.

[29] V. Mohanavel, K. R. Kumar, T. Sathish, P. Velmurugan, A. Karthick, M. Ravichandran, S. Alfarraj, H. S. K. Almoallim, S. Kumar, and I. J. R. Lalvani, "Investigation on inorganic salts K_2TiF_6 and KBF_4 to develop nanoparticles based TiB_2 reinforcement aluminium composites," *Bioinorganic Chemistry and Applications*, vol. 2022, no. 3, p. 8559402, 2022.

[30] J. D. R. Selvam, D. S. R. Smart, and I. Dinaharan, "Microstructure and some mechanical properties of fly ash particulate reinforced AA6061 aluminum alloy composites prepared by compocasting," *Materials and Design*, vol. 49, pp. 28–34, 2013.

[31] S. Suresh, N. S. V. Moorthi, and C. E. Prema, "Tribological and mechanical behavior study of Al6061-TiB_2 metal matrix composites using stir casting," *Advanced Materials Research*, vol. 984–985, pp. 200–206. 2014.

[32] M. Z. Khan, M. Anas, A. Hussain, M. Irshadul Haque, and K. Rasheed, "Effect on mechanical properties of aluminium alloy composites on adding ash as reinforcement material," *Journal of Metals Materials and Minerals*, vol. 25, no. 2, pp. 1–7, 2015.

[33] N. Kumar, R. K. Gautam, and S. Mohan, "In-situ development of ZrB_2 particles and their effect on microstructure and mechanical properties of AA5052 metal-matrix composites," *Materials and Design*, vol. 80, pp. 129–136, 2015.

[34] K. Ravikumar, K. Kiran, and V. S. Sreebalaji, "Characterization of mechanical properties of aluminium/tungsten carbide composites," *Measurement*, vol. 102, pp. 142–149, 2017.

[35] S. Suresh, and N. S. V. Moorthi, "Process development in stir casting and investigation on microstructures and wear behavior of TiB_2 on A16061 MMC," *Procedia Engineering*, vol. 64, pp. 1183–1190, 2013.

[36] M. Madhusudhan, G. J. Naveen, and K. Mahesha, "Mechanical characterization of AA7068-ZrO_2 reinforced metal matrix composites," *Materials Today: Proceedings*, vol. 4, no. 2, pp. 3122–3130, 2017.

[37] B. P. Nagasai, C. H. Anusha, and A. Rajesh, "Study on mechanical properties of Al-6061/ZrO_2 reinforced metal matrix composites," *Materials Today: Proceedings*, vol. 47, pp. 4552–4557, 2021.

[38] J. Johnson, and R. Raja, "Evaluation of the effect of strontium and tungsten carbide on the microstructure evolution, tribological and mechanical behaviour of Al-Zn-Mg-Cu-5Sr-WC metal matrix composite," *Journal of Metals, Materials and Minerals*, vol. 34, no. 2, pp. 1–13, 2024.

[39] S. A. Farooq, S. H. Mukhtar, A. Raina, M. I. U. Haq, Md. I. H. Siddiqui, N. Naveed, and D. Dobrota, "Effect of TiB_2 on the mechanical and tribological properties of marine grade aluminum alloy 5052: An experimental investigation," *Journal of Materials Research and Technology*, vol. 29, pp. 3749–3758, 2024.

[40] D. S. E. J. Dhas, C. Velmurugan, K. L. D. Wins, and K. P. BoopathiRaja, "Effect of tungsten carbide, silicon carbide and graphite particulates on the mechanical and microstructural characteristics of AA 5052 hybrid composites," *Ceramics International*, vol. 45, no. 1, pp. 614–621, 2019.

[41] P. Natarajan, T. Sekar, V. Chenrayan, and L. Rajeshkumar, "The effect of SiC and Y_2O_3 inclusion on microstructure and mechanical properties of Al 5052 composite fabricated through friction stir process," *Heliyon*, vol. 11, no. 1, 2025.

[42] K. R. Kumar, K. Kiran, and V. S. Sreebalaji, "Microstructural characteristics and mechanical behaviour of aluminium matrix composites reinforced with titanium carbide," *Journal of Alloys and Compounds*, vol. 723, pp. 795–801, 2017.

[43] D. A. Tirfe, A. Alemayehu, M. Ewnetu, B. R. Hunde, and A. D. Woldeyohannes, "Optimizing the impact toughness of stir-casted bamboo leaf stem ash reinforced aluminum matrix composite using Taguchi method," *Next Materials*, vol. 9, p. 101025, 2025.